EUROFUSION WPMST1-PR(16) 16203

N Leuthold et al.

Parameter dependence of ELM loss reduction by magnetic perturbations at low pedestal density and collisionality in ASDEX Upgrade

Preprint of Paper to be submitted for publication in
Plasma Physics and Controlled Fusion

This work has been carried out within the framework of the EUROfusion Consortium and has received funding from the Euratom research and training programme 2014-2018 under grant agreement No 633053. The views and opinions expressed herein do not necessarily reflect those of the European Commission.

Parameter Dependence of ELM Loss Reduction by Magnetic Perturbations at low Pedestal Density and Collisionality in ASDEX Upgrade

N Leuthold[1], W Suttrop[1], R Fischer[1], A Kappatou[1,2], A Kirk[3], R McDermott[1], A Mlynek[1], M Valovič[3], M Willensdorfer[1], the ASDEX Upgrade Team[1] and the EUROfusion MST1 Team[4]

[1]Max Planck Institute for Plasma Physics, 85748 Garching, Germany
[2]FOM Institute DIFFER, De Zaale 20, 5612 AJ Eindhoven, Netherlands
[3]CCFE, Culham Science Centre, Abingdon, Oxon, OX14 3DB, U.K.

E-mail: nils.leuthold@ipp.mpg.de

Abstract. ELM mitigation by magnetic perturbations is studied at ITER-like low pedestal collisionalities ($\nu^*_{\mathrm{PED}} = 0.1 - 1$) in ASDEX Upgrade. A comprehensive database of ELM energy losses for varying plasma density, heating power, edge safety factor and magnetic perturbation structure has been assembled to investigate parameter dependencies of ELM mitigation. It is found that magnetic perturbations with a toroidal mode number $n = 2$ can reduce the ELM energy loss normalized to the energy stored in the plasma pedestal from about 30% to less than 5%, i.e. by a factor of six, below an electron pedestal collisionality of $\nu^*_{\mathrm{e,PED}} = 0.4$. At this level of ELM mitigation a significant reduction of the pedestal pressure and, therefore, global plasma confinement occurs. This pedestal pressure reduction is mostly due to a reduction of plasma density, the so-called "pump-out" effect. Refueling by neutral beams and in particular by pellet injection is possible and can re-establish confinement, however, the ELM energy loss increases as well.

1. Introduction

Edge Localized Modes (ELMs) appear in high-confinement modes (H-modes) [1] as a consequence of the transport barrier at the plasma edge, which allows the edge pressure gradient to increase (and form the so-called "edge pedestal") until a stability limit for ELMs is reached. ELMs cause rapid heat and particle loss from the confined plasma which can flush impurities out but also leads to very strong heat loads on plasma facing components. Various studies have attempted extrapolations of the ELM-related divertor heat load to ITER [2, 3, 4, 5] and assuming that plasma collisionality is the ordering parameter for the ELM size it appears necessary to mitigate ELM losses by a large factor or suppress ELMs altogether. Recently, a root dependence of the ELM energy loss on the pedestal pressure was found in a database containing JET, MAST and ASDEX Upgrade data, also predicting the necessity to mitigate or suppress ELMs at ITER [6]. Weak non-axisymmetric perturbations of the tokamak magnetic field have proven to be an efficient method of ELM mitigation [7, 8, 9] or suppression [10, 11] and have therefore become an important branch of current research.

In 2010 ASDEX Upgrade has been upgraded with two sets of 8 in-vessel saddle coils [12, 13], which are distributed toroidally above and below the outer midplane (Fig.1), allowing magnetic perturbations

[4] www.euro-fusionscipub.org/mst1

of the plasma surface with toroidal mode numbers of up to $n = 4$. Their radial non-axisymmetric magnetic field is weak compared to the toroidal field ($B_{MP} \approx 10^{-3} \cdot B_t$). With this setup ELM mitigation experiments via magnetic perturbation initially target plasmas with high pedestal collisionality ($\nu^*_{\mathrm{PED}} > 1$) [9, 14, 15]. A reduction of the ELM energy loss and divertor heat load was achieved for a wide range of edge safety factor ($q_{95} = 4.0 - 6.5$) above a certain critical threshold of the edge electron density. This threshold was found to be plasma current dependent and it can, therefore, be expressed as a fraction of the Greenwald density, $(0.6 - 0.65) \cdot n_{GW}$, where $n_{GW} = I_p/(\pi a^2)$ is the Greenwald density in $10^{20}\mathrm{m}^{-3}$, a the minor radius in m, and I_p the plasma current in MA. Also an effect of the MP coils on the edge density can be found, namely a slight increase for resonant MP fields or decrease at minimum resonance [16]. While the density variation seems to depend on the field structure of the perturbation, the ELM mitigation effect itself appears to be practically independent of it [9]. During the mitigated phases the confinement is preserved and the core tungsten concentration is reduced. Later on, a quite distinct regime of ELM mitigation at low pedestal collisionality ($\nu^* < 0.5$) was explored in ASDEX Upgrade for $n = 1,2,4$ magnetic perturbations [17, 18, 19]. In contrast to the high collisionality regime, ELM mitigation is found to strongly depend on the perturbation field structure at low pedestal collisionality. Also, the plasma density is reduced as the magnetic perturbation is applied, which is a common observation in various experiments [20] and has been dubbed the "density pump-out". The plasma response was found to depend on the alignment of the applied magnetic perturbation with the background plasma magnetic field [19, 21] which can be varied by adjusting the phase difference $\Delta\phi$ between upper and lower coil ring ("differential phase"). In agreement with ideal MHD predictions by MARS-F [22], NEMEC [23], and JOREK [24] codes, the strongest plasma response occurs when the field is aligned such as to couple to the edge pressure gradient driven stable ideal kink mode. In the plasmas investigated the magnetic perturbation has the strongest amplitude of the components at $m = q \cdot n + 2$, which is distinctly offset from field alignment by a poloidal mode number shift of $\Delta m = 2$ [25, 24]. Additional effort was made to achieve even lower collisionality ($\nu^* < 0.2$) close to ITER operation values. In this work, data from all low collisionality experiments on ELM mitigation at ASDEX Upgrade is combined to study the influence of pedestal plasma parameters on the loss of stored energy caused by ELMs. The paper is structured as follows. In section 2 the dataset and its scope are described. Sections 3 and 4 motivate the normalization of the ELM energy losses to the energy stored in the pedestal and describe the dependency of normalized ELM loss on pedestal parameters. The results are discussed in sections 5 and 6.

2. Plasma Parameters for ELM Mitigation Experiments

In these experiments, H-mode plasmas are produced in lower single null (LSN) configuration with plasma current $I_p = 0.8$MA. All plasmas have low triangularity (upper $\delta_u = 0.053 - 0.192$ and lower $\delta_l = 0.460 - 0.546$). Details of these experiments are described in Ref. [19]. We consider two main classes of discharges, those at low edge safety factor $q_{95} \approx 3.6 - 3.9$ and high edge safety factor $q_{95} \approx 5.1 - 5.4$ corresponding to a toroidal magnetic field $B_t = 1.8$T and 2.5T, respectively. Magnetic perturbations with a toroidal mode number $n = 2$ and variable amplitude (perturbation coil current) and poloidal spectrum are produced. The poloidal spectrum is varied by variation of the differential phase. These plasmas are heated with up to 10MW neutral beam injection power and about 3MW electron cyclotron heating at $f = 140$GHz, which is centrally deposited in second or third harmonic in the case of the high and low q_{95} scenarios, respectively. Centrally deposited heating power has been found to be essential in order to maintain net outflux of heavy impurities, especially tungsten impurities produced by sputtering from the all-tungsten plasma facing components in the ASDEX Upgrade main chamber. In order to allow access to lowest pedestal collisionalities down to $\nu^*_{\mathrm{PED}} \sim 0.1$, little or no gas puff is applied. Fresh boronisation has been found instrumental to increase wall pumping from a large surface area and to reduce tungsten sputtering from auxiliary limiters in the main chamber, the main sources of heavy impurities in the plasma.

A total of 20 discharges are used to build a dataset that allows to study the dependence of the energy losses ΔW_{ELM} caused by ELMs on plasma parameters, especially at the H-mode pedestal. Time intervals

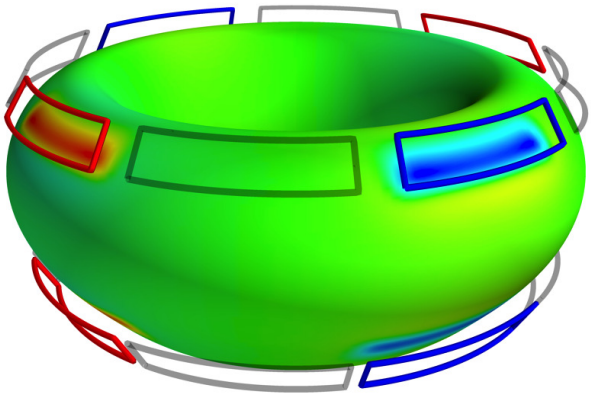

Figure 1. Schematic illustration of the 16 magnetic perturbation coils in ASDEX Upgrade. The green vacuum background is perturbed by the small, radial field created by the powered external field coils shown in red and blue with opposite sign. [21]

of 100ms duration are identified and averages of ΔW_{ELM} as well as the pedestal parameters are taken in these intervals. Electron density and temperature profiles are obtained by integrated data analysis [26], which takes into account several diagnostics for each quantity. This includes interferometry [27] and lithium beam diagnostic [28] for the electron density and electron cyclotron emission [29, 30] for the electron temperature. The latter is restricted by X-mode wave cut-off and low optical depth at very high or low densities, respectively, and therefore Thomson scattering data [31, 32] is in some cases added as well. Charge exchange recombination spectroscopy [33] is used to measure ion temperature profiles as well as the impurity content. ΔW_{ELM} is defined as the difference of stored energy before and after the ELM crash. The equilibrium reconstruction by function parametrization yields the stored energy. The smallest ELMs achieved fall below the noise level of the stored energy, which is about $6-8$kJ.

The distribution of ELM losses often exhibits two distinct peaks at very different ELM loss energy (see Fig. 2). Since, in the presence of an erosion threshold, the largest ELMs have the highest damage potential in terms of peak heat loads and target erosion rates, we consider the average ELM loss of only those ELMs with losses above 50% of the maximum ELM loss in a time interval. This threshold is indicates by the black line in Fig. 2. ELMs with losses smaller than 50% of the maximum are ignored. This dataset covers a wide range of pedestal parameters and ELMs with an energy loss between 0 and 70kJ. The electron pedestal density covers the range from 1.5 to $6.0 \cdot 10^{19}\mathrm{m}^{-3}$ corresponding to about 15 to 60% of the Greenwald density. The pedestal electron temperature varies between 0.25 and 1.5keV, while ions can be hotter than electrons and cover the range from 0.25 to 1.9keV. The pressure of the electrons at the pedestal top ranges from 1 to 9kPa and electron collisionalities between 0.09 and 3 were achieved. For the calculation of the collisionality the impurity content is measured directly by charge exchange recombination spectroscopy (CXRS) for helium and boron. Carbon and nitrogen concentrations, intrinsic levels of which are very low in ASDEX Upgrade with all-metal plasma facing components, are estimated from line intensities relative to the measured boron. The differences in the charge exchange cross-sections are taken into account by using a constant factor, corresponding to the first energy component of the neutral beam. Fig. 3 (left) shows the effective ion charge fraction ΔZ_{eff} of each impurity at the pedestal top which contribute to the effective ion charge [34]

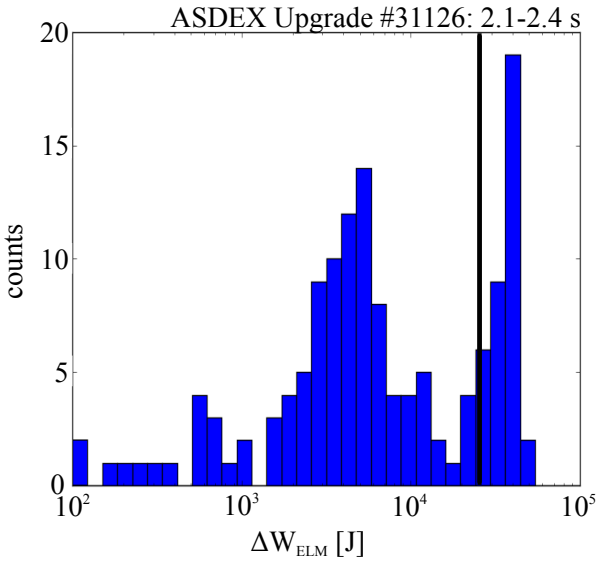

Figure 2. Histogram of the ELM energy loss ΔW_{ELM} during an representative discharge with coexisting small and large ELMs. The black line indicates about 50% of the maximum ELM in this time interval.

$$Z_{eff} = \frac{\sum_i n_{i,PED} \cdot Z_i^2}{n_{e,PED}} \tag{1}$$

as a function of the electron pedestal density. Here, $n_{i,PED}$ is the ion pedestal density in m^{-3}, Z_i the charge, $n_{e,PED}$ the electron pedestal density in m^{-3} and i are the different impurities. After the wall conditioning using a diborane glow discharge in He carrier gas, these two impurities are dominant; however helium does not strongly contribute to Z_{eff}. Carbon and nitrogen are comparable to each other and contribute to Z_{eff} significantly, especially at higher electron density. Unfortunately, N and C were not routinely measured in this dataset and, therefore, only helium and boron are considered to keep consistency. Fig. 3 (right) shows that $\nu^*_{e,PED}$ in the reduced dataset is consistent with calculations including also nitrogen and carbon within the error bars.

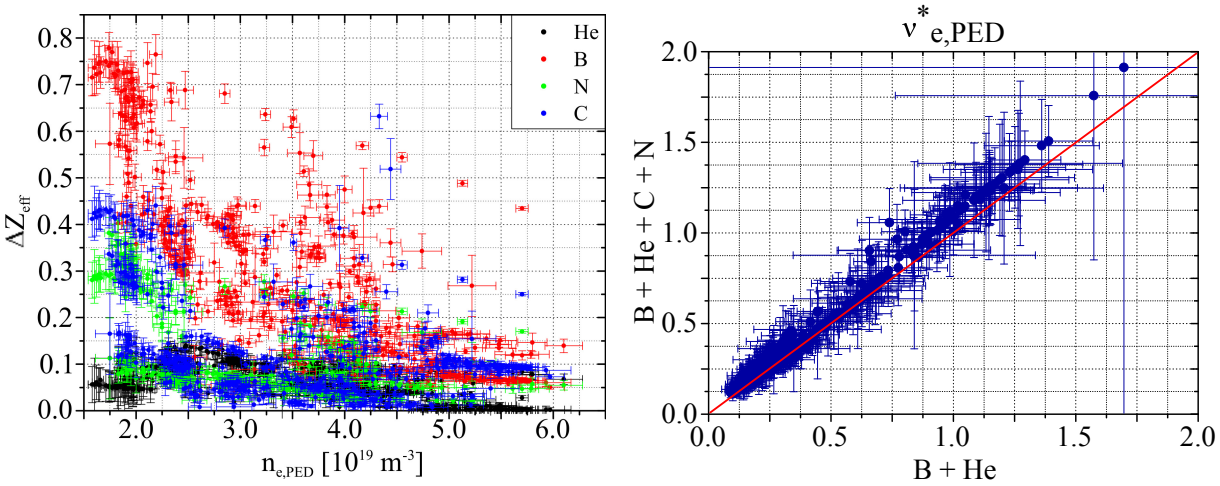

Figure 3. Left: ΔZ_{eff} fraction of helium, boron, nitrogen and carbon plotted as a function of the electron pedestal density. Right: Comparison of $\nu^*_{e,PED}$ including also carbon and nitrogen with the reduced dataset consisting only of helium and boron.

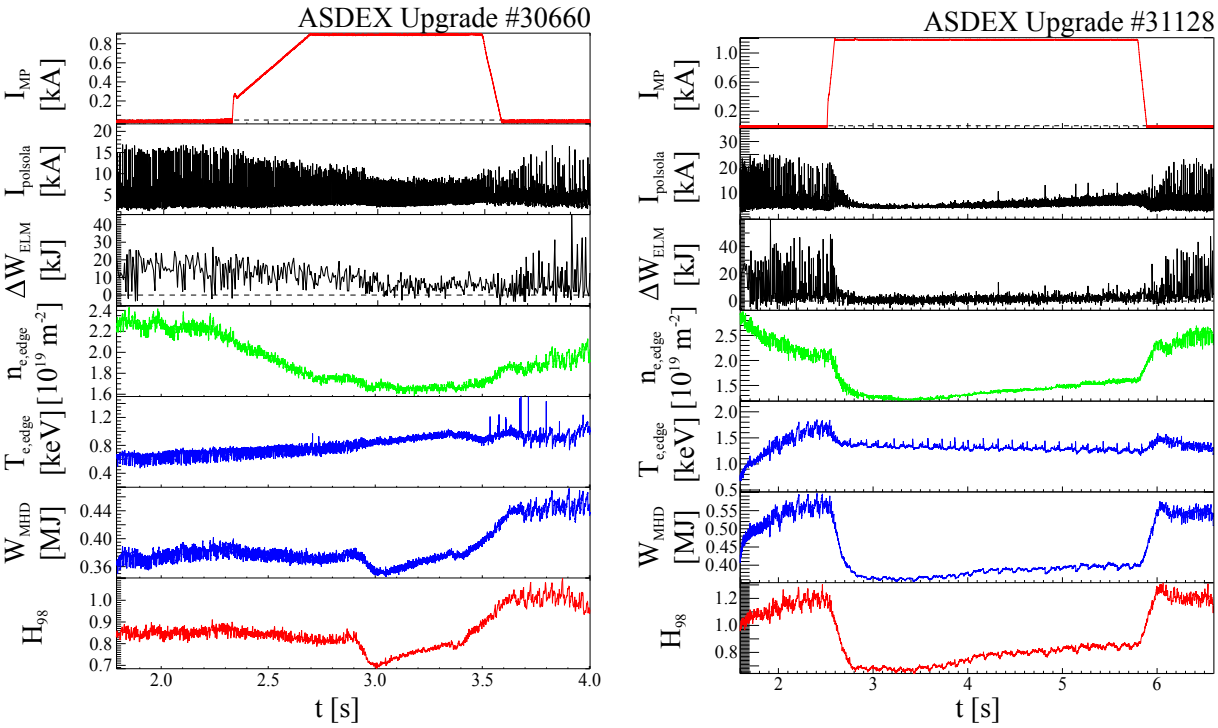

Figure 4. Time traces of high q_{95} discharge #30660 and low q_{95} discharge #31128 showing the ELM mitigation and density pump-out effect. Here, I_{MP} is the current in the magnetic perturbation coils, $I_{polsola}$ the poloidal thermocurrent measured in the outer divertor target, ΔW_{ELM} the absolute ELM energy loss, $n_{e,edge}$ the line integrated density close to the pedestal top, $T_{e,edge}$ the electron temperature close to the pedestal top, W_{MHD} the energy stored in the plasma and H_{98} the confinement time relative to ITER IPB98(y,2) scaling [35].

3. ELM Mitigation and Plasma Behavior

In Fig. 4 time traces are shown of discharges that exhibit ELM mitigation, pulse 30660 with high $q_{95} \approx 5.1$ (left) and pulse 31128 with low $q_{95} \approx 3.8$. As the perturbation coil current is ramped up, two effects become apparent in both discharges: (i) A pronounced reduction of plasma density, the so-called "density pump-out" effect, which is in some cases accompanied by lower pedestal temperature and generally leads to a reduced pedestal pressure and consequently reduce plasma confinement. (ii) The desired mitigation of the ELMs which can be seen in the time traces of the thermocurrent measured in the outer divertor $I_{polsola}$, which is indicative of the divertor heat load by ELMs as well as the ELM energy loss ΔW_{ELM} from the main plasma. The degree of ELM mitigation is quite different in these two discharges and varies in fact in the entire dataset. We now venture to find parameters that can describe ELM losses and the degree of ELM loss mitigation empirically. Since ELM stability is governed by edge pedestal parameters and ELM losses affect predominantly the plasma edge, we naturally focus on edge pedestal parameters such as electron density, electron and ion temperature, electron pressure, and electron collisionality as possibly relevant parameters.

As the heat outflux due to ELMs originates from a brief collapse of the H-mode edge barrier it is natural to expect that the ELM energy loss will depend on the kinetic plasma energy stored in this region, which is a fraction of the energy stored in the plasma pedestal ("pedestal energy")

$$W_{PED} = \frac{3}{2} \cdot V \cdot (n_{e,PED} \cdot T_{e,PED} + n_{i,PED} \cdot T_{i,PED}) \tag{2}$$

where V is the plasma volume in m^3, $T_{e,PED}$ the electron pedestal temperature in eV, $T_{i,PED}$ the ion

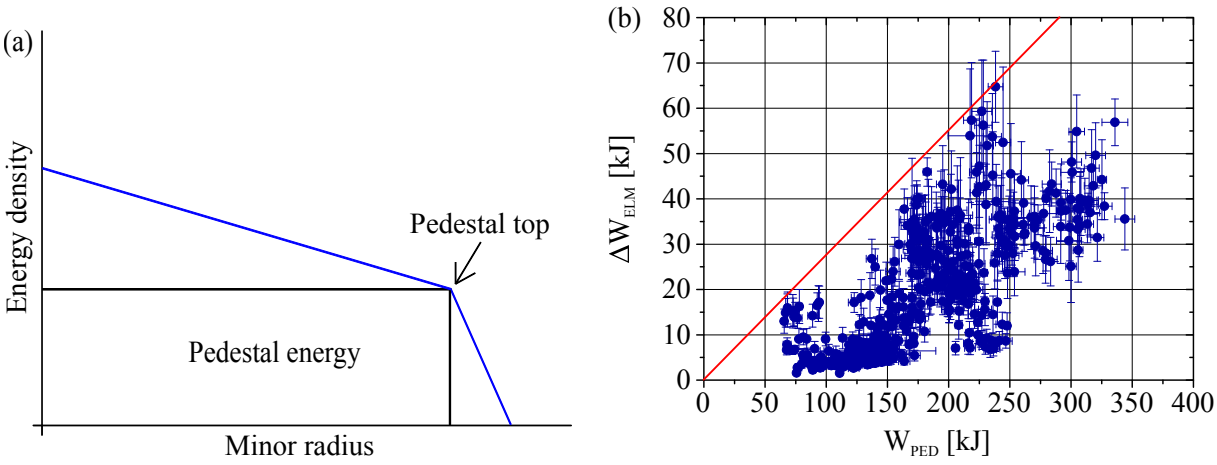

Figure 5. (a) Schematic illustration of the pedestal stored energy W_{PED}. (b) Absolute ELM energy loss ΔW_{ELM} as a function of the pedestal stored energy W_{PED}. The red line indicates a constant fraction $\Delta W_{ELM}/W_{PED}$ of 0.27.

pedestal temperature in eV, $n_{e,PED}$ the electron pedestal density in m^{-3}, and $n_{i,PED}$ the ion density in m^{-3} approximated as:

$$n_{i,PED} = n_{D,PED} + n_{B,PED} + n_{He,PED} \tag{3}$$

$n_{B,PED}$ is the boron density in m^{-3}, $n_{He,PED}$ the helium density in m^{-3}, and $n_{D,PED}$ the deuterium density in m^{-3}. The boron and helium density are measured directly by CXRS, while the deuterium density is approximated by the remaining electron content (assuming total ionization at the pedestal top). As it can be seen from the cartoon in the left part of Fig. 5, the pedestal energy is a fraction of the total stored kinetic plasma energy governed by the edge pedestal top pressure (related to the energy density). The maximum ELM energy loss in our dataset (including unmitigated and mitigated ELMs) is indeed capped by a limit which can be described as a fraction of pedestal stored energy, as can be seen on the right side of Fig. 5. The red line is at a constant fraction of $\Delta W_{ELM}/W_{PED} = 0.27$, which indicates an upper limit for the ELM energy losses. Subsequently, we stick with the normalized ELM energy loss $\Delta W_{ELM}/W_{PED}$ and examine the parameter dependence of this quantity. The four main data classes are distinguished by a color-code, low q_{95} with (red) and without (black) magnetic perturbation and high q_{95} with (orange) and without (blue) magnetic perturbation.

We first focus on the question whether ELM losses (unmitigated and mitigated) and the access condition for ELM mitigation can be described by the plasma collisionality, e.g. the pedestal electron collisionality ([36]):

$$\nu^*_{e,PED} = 6.921 \cdot 10^{-18} \cdot \frac{n_{e,PED}}{T^2_{e,PED}} \cdot (R \cdot q_{95}) \cdot Z_{eff} \cdot \varepsilon^{-3/2} \cdot \ln(\Lambda_e) \tag{4}$$

Here, $n_{\mathrm{e,PED}}$ is the electron pedestal density in m^{-3}, $T_{\mathrm{e,PED}}$ the electron pedestal temperature in eV, R the major radius in m, q_{95} the edge safety factor, Z_{eff} the effective ion charge at the plasma edge, ε the inverse aspect ratio, and $\ln(\Lambda_e)$ the Coulomb logarithm. Ions taken into account for Z_{eff} are boron and helium as described in section 2, carbon and nitrogen are ignored. Consequently, the $\nu^*_{e,PED}$ calculated in this paper is lower than in reality. In Fig. 6 (a) a threshold can be seen at about $\nu^*_{\mathrm{e,PED}} \approx 0.4$, which divides the data in two subsets. In the region with lower collisionality the best degree of ELM mitigation is obtained with magnetic perturbation: The ELM energy loss is reduced to $2.5 - 7.5\%$ of the pedestal stored energy at $\nu^*_{e,PED} = 0.09$ to 0.4. The discharges in this collisionality range are for the most part those with a low edge safety factor. In case of higher collisionality, only phases with ELM losses at

$\Delta W_{\mathrm{ELM}}/W_{\mathrm{PED}} > 7.5\%$ or higher are observed. In this region the ELM energy loss is up to nearly a third of the pedestal stored energy and the majority of data show an increasing trend with the collisionality. This region comprises most of the pulses at higher q_{95}, and hence increased collisionality, but also some pulses with low q_{95}. Since several discharges with higher edge safety factor and an electron pedestal collisionality of about $0.2-0.4$ also show normalized ELM energy losses in the region of $5-10\%$, we conclude that a high degree of ELM mitigation is not limited to low q_{95} per se, but can be achieved with higher q_{95} if the pedestal collisionality (or a related parameter) is kept sufficiently low.

Inspection of our present comprehensive dataset on ELM mitigation pulses in ASDEX Upgrade reveals that the pedestal plasma density itself is an ordering parameter for ELM losses, surprisingly irrespective of the presence of magnetic perturbations. In Fig. 6 (b) one sees that the lowest ELM energy losses are achieved at lowest density with magnetic perturbation switched on in the low edge safety factor case. Apart from that, the dataset shows a clear trend with density, i.e. the normalized ELM energy loss increases with increasing density. This trend comprises all data with and without magnetic perturbation and at any edge safety factor. The existence of outliers with high safety factor and above-average ELM losses at pedestal densities around $3-4\times10^{19}\mathrm{m}^{-3}$ indicate that there are probably other yet unidentified, hidden parameters, which still have to be quantified.

In contrast, Figs. 6 (c) and (d) demonstrate that neither electron temperature nor ion temperature, respectively, at the pedestal correlate well with the normalized ELM energy loss. Cases both with ELM mitigation by magnetic perturbations and without are spread over the entire temperature range from $0.25-1.5$keV (electrons) and $0.25-1.9$keV (ions).

One may suspect that the electron density enters through correlation with the pedestal pressure which is in turn related to the edge pressure gradient that drives the ELM instability. We therefore consider the dependence of the normalized ELM energy loss $\Delta W_{\mathrm{ELM}}/W_{\mathrm{PED}}$ (Fig. 6 (e)) and absolute ELM energy loss ΔW_{ELM} (Fig. 6 (f)). The ELM energy loss ΔW_{ELM} does indeed correlate with pedestal pressure, as already shown in Fig. 5 and this is the basis for the choice of normalization. The normalized, residual ELM energy loss $\Delta W_{\mathrm{ELM}}/W_{\mathrm{PED}}$, however, does not show better correlation with pedestal pressure than with pedestal density, i.e. the scatter of Fig. 6 (b) is not due to the temperature variation shown in Figs. 6 (c) and (d).

The relative importance of the above candidate parameters can be assessed by inspecting Spearman's correlation coefficient [37], which tests non-linear correlations varying from -1 (perfect anti-correlation) through 0 (no correlation) to 1 (perfect correlation) and is not very sensitive to few outliers. The resulting coefficients for the correlation between the ELM energy loss normalized to the pedestal stored energy and each pedestal parameter are shown in Table 1. As expected, the best correlation exists with the pedestal plasma density. However, significant scatter in the data – above uncertainties – leads to the expectation that additional hidden parameters may play a role.

Pedestal parameter:	$T_{i,PED}$	$T_{e,PED}$	$p_{e,PED}$	$\nu^*_{e,PED}$	$n_{e,PED}$
r_S	-0.45	-0.44	0.43	0.50	0.79

Table 1. Spearman's correlation coefficients for the correlation between the normalized ELM energy loss and each pedestal parameter.

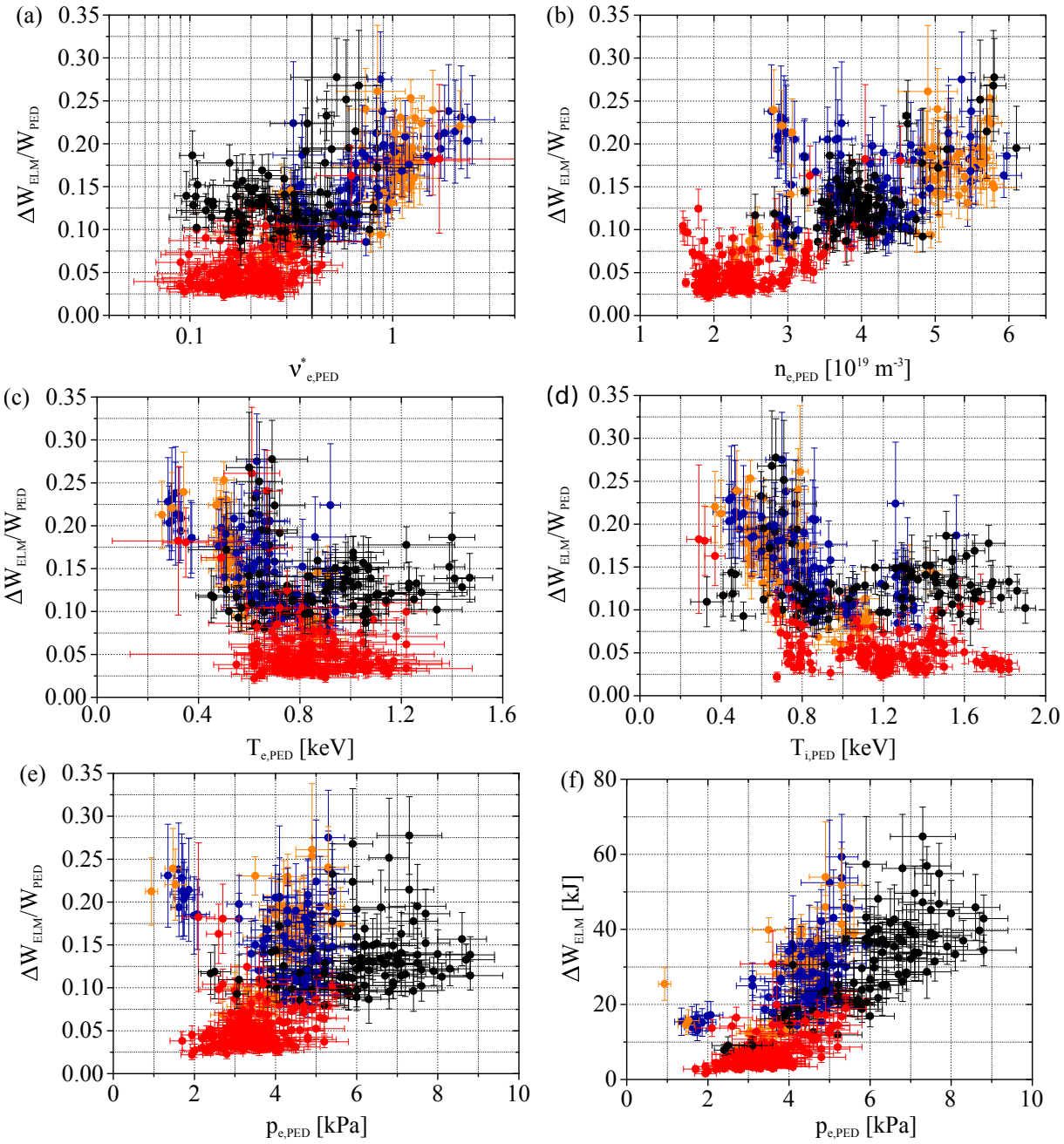

Figure 6. The normalized ELM energy loss plotted against the (a) electron pedestal collisionality, (b) electron pedestal density, (c) electron pedestal temperature, (d) ion pedestal temperature, and (e) electron pedestal pressure. (f) shows the absolute ELM energy loss as a function of the electron pedestal pressure. The dataset consists of discharges with magnetic perturbation (● low edge safety factor, ● high edge safety factor) and without magnetic perturbation (● low edge safety factor, ● high edge safety factor).

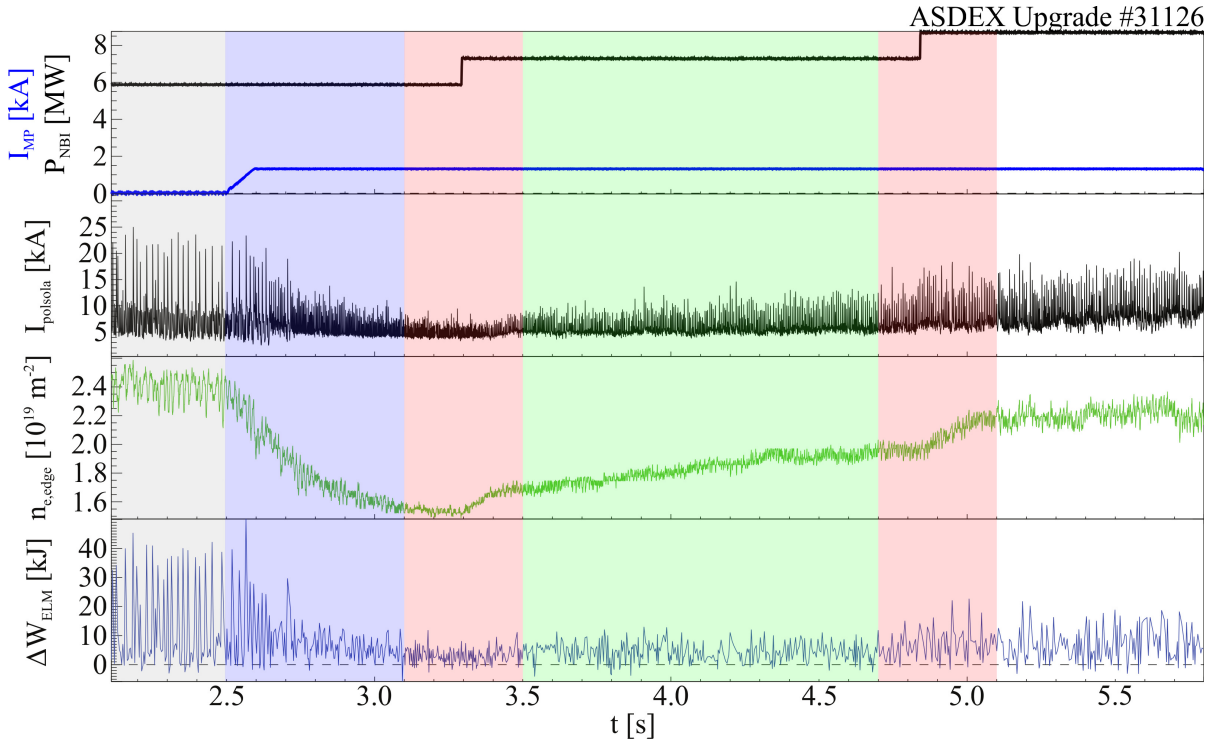

Figure 7. Time traces of a typical ELM mitigation discharge at low collisionality. Highlighted are phases where the evolution of the ELMs is similar to the electron edge density evolution, but with different influences.

4. Comparison of Techniques to vary the Plasma Density

Now the role of different methods to modify the plasma density and their effect on ELM losses is investigated: Density "pump-out" by magnetic perturbations with varying poloidal spectrum, injection of deuterium pellets and variations of neutral beam heating power. In this context it is useful to examine individual discharges in more detail. If the plasma density or a parameter directly dependent on the plasma density is governing the ELM losses, they should show the same dependence on density independently of how the variation was obtained.

Pump-out and varying neutral beam injection heating

In discharge #31126 a strong variation of the density is achieved by a step-wise increase of the neutral beam heating power while a resonant magnetic perturbation is applied. Fig. 7 shows characteristic time traces of this pulse: neutral beam heating power P_{NBI}, MP coil current I_{MP}, outer divertor SOL thermocurrent I_{polsola}, peripheral line integrated density $n_{\mathrm{e,edge}}$, and ELM loss energy ΔW_{ELM}. Several time intervals are marked up in the figure which will be discussed subsequently. The first phase up to $t = 2.5$s (grey background) is a reference phase just before the magnetic perturbation is applied, with largest plasma density and largest ELM loss energies. After $t = 2.5$s, the magnetic perturbation is applied. This phase has the largest ELMs turn gradually into small ELMs while the plasma density drops until $t = 3.1$s (blue background). In Fig. 8, the time scales of the density decay and of the ELM signal decays are compared: An exponential fit to the decay of those signals yields a time constant of $\tau_n = [249.3 \pm 1.8]$ ms for the density, $\tau_{DC} = [270 \pm 3]$ ms for the divertor current and $\tau_{ELM} = [245 \pm 48]$ ms for the normalized ELM energy loss. One can see that the evolution times of all signals are of the same order, though, the fit of the normalized ELM loss signal has huge uncertainties. This supports the suspicion that the ELM energy loss correlates with the electron pedestal density. The time intervals

$t = 3.1 - 3.5$s and $t = 4.7 - 5.3$s (red background in Fig. 7) demonstrate the effect of increasing the neutral beam heating power in steps which each lead to an increase of the electron edge density. Simultaneously the peak divertor thermocurrent and ELM energy loss show an increase with a time constant of about 100ms. During the time interval $t = 3.5 - 4.7$s (second green background in Fig. 7) heating power and MP coil current are held constant, however, the plasma density creeps up slowly, accompanied by a similarly slow increase of divertor thermocurrent. Most likely because of the uncertainties in the calculation of the energy loss and the only very slight and slow increase of the density, this increase dies out in the scattering for the ELM energy loss. The original density pump-out after MP application, neutral beam fueling and slow evolution of the recycling particle flux all lead to a concomitant change of ELM loss energy.

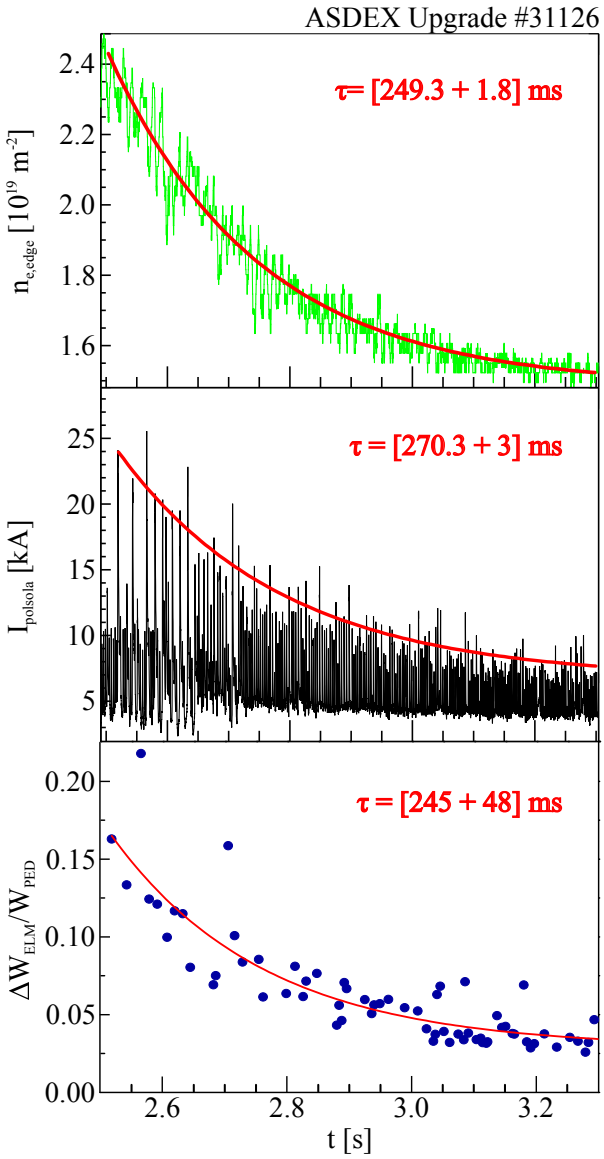

Figure 8. Comparison of the evolution of the density and ELMs right after switching on the magnetic perturbation at $t = 2.5$s for discharge #31126. Exponential fit to the line integrated electron density at $\rho_{pol} = 0.88$ (top), divertor current (middle) and normalized ELM energy loss (bottom).

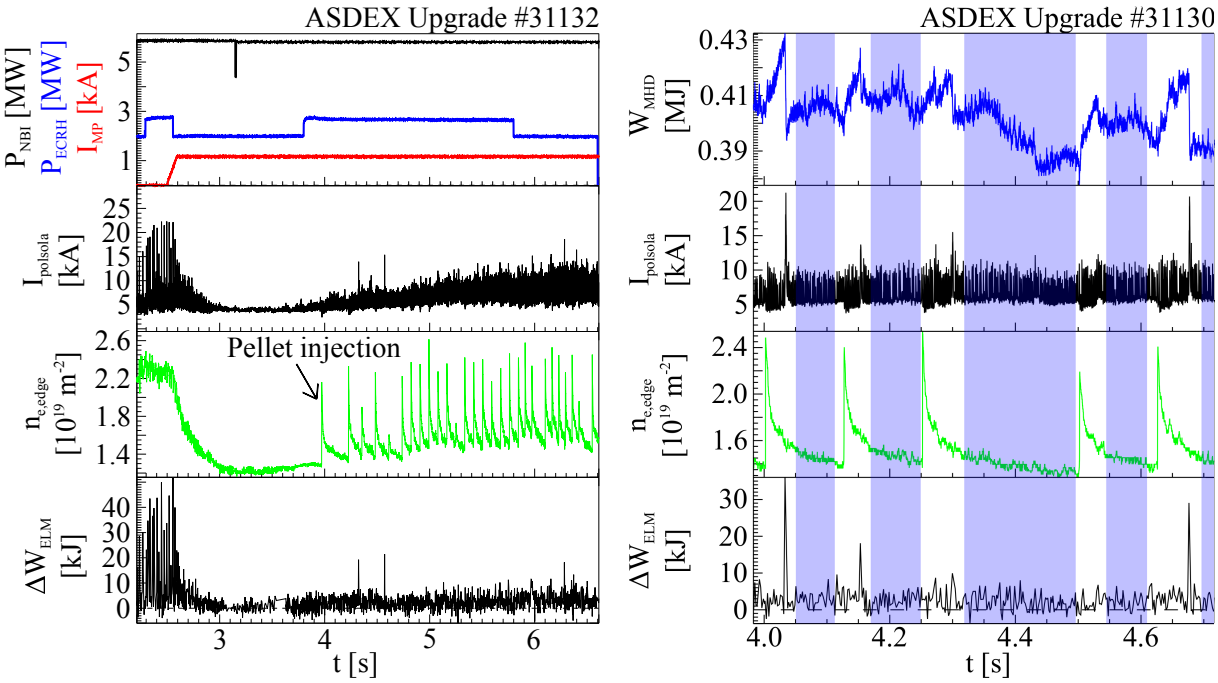

Figure 9. Left: Time traces of discharge #31132 with injection of deuterium pellets starting at $t = 4$s. Right: Time traces of discharge #31130 during pellet injection with the evaluated time intervals being highlighted.

Pellet injection

Significant fueling can be provided by deuterium pellet injection [38]. The simultaneous application of pellet injection and magnetic perturbation has been studied before with the aim to increase confinement, while keeping ELMs mitigated [39, 40]. In Ref. [39], in fact a recovery of the core density was demonstrated. The edge density rises quickly as each individual pellet is injected, but drops again before arrival of the subsequent pellet, so that both the baseline and average edge densities remain below the reference value without pellets. In discharge #31132 (see left side of Fig. 9), ELM mitigation and density "pump-out" are initially observed after application of the MP, before the injection of deuterium pellets (1.4 x 1.5 x 1.5mm, $N_{pel} = 1.2 \cdot 10^{20}$ atoms) starts at $t = 4$s. Each pellet leads to a sudden rise of the plasma density, but because of the quick decay in between pellets, their repetition frequency has to be increased from 7.5Hz to 12Hz at 4.7s and finally 15Hz at 5.85s is needed for further fueling. Those adjustments allow the minimum density in between pellets to increase over time, indicating partial refueling (in the interval from $t = 4$ to 6.6s) of the pedestal density. The ELM frequency (not shown) decreases and ΔW_{ELM} as well as $I_{polsola}$ increase with density. Note that ELMs are not directly triggered by the injected pellets, unlike the observations in ELMy H-mode without magnetic perturbation [38]. When comparing the inter-pellet data (green symbols) to the density dependence of the normalized ELM loss energy in the full dataset (black symbols) (Fig. 10) the same density dependence becomes apparent. The data used in this comparison was obtained during phases between single pellet injections after the pedestal density has stabilized again. But directly after the pellet injection when the pedestal density is increased for a short time to the density level before the magnetic perturbation, one would expect the ELM losses to be comparable to the pre MP ELM losses. Yet, the ELMs seem to not be affected by this short time change in the pedestal density. Instead, large ELMs occur sometimes several ms after the peak density has occurred, at a time when the density has decayed already (see right side of Fig. 9). Such infrequent, large ELMs are harmful in the presence of an ablation threshold of the divertor material. The reason for their appearance is not known yet.

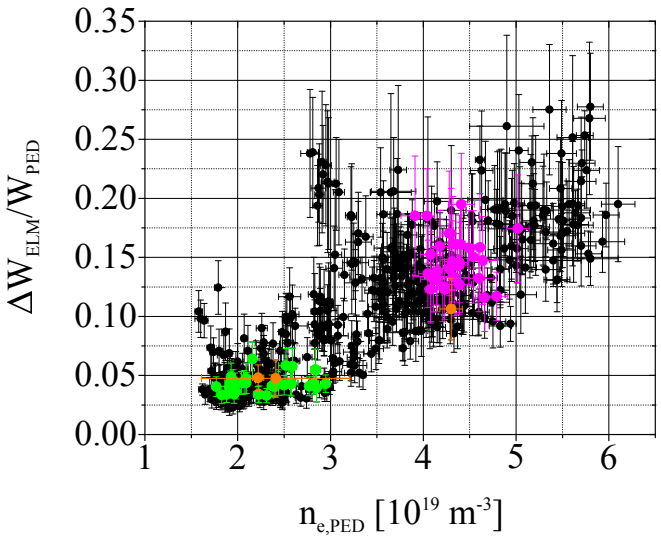

Figure 10. The normalized ELM energy loss plotted against the electron pedestal density including the discharges with pellet injection and $\Delta\phi$ scan. In ● are all the data shown in section 3 and highlighted are the data ● with pellet injection, ● during a $\Delta\phi$ scan at high q_{95} and ● during a $\Delta\phi$ scan at low q_{95}.

Varying poloidal spectrum of the magnetic perturbation

Finally, we study the effect of varying alignment of the magnetic perturbation with the plasma magnetic field on plasma density and ELM loss. It has been observed before that the strength of the density reduction depends on the degree of coupling of the external perturbation field to ideal modes that are amplified by the edge pressure gradient and edge current density rather than geometrical alignment of the perturbation with the magnetic field line pitch in the edge plasma [41, 19]. For the case of the ASDEX Upgrade MP coil set, this condition is directly governed by the differential phase $\Delta\phi$ between the upper and lower coil rings. The dependence of the plasma response on the differential phase $\Delta\phi$ is clearly visible in pulses with temporal variation (scans) of $\Delta\phi$. Fig. 11 shows time traces of pulse #30682 at low edge safety factor, $q_{95} \approx 3.7$. The magnetic perturbation is on until $t = 1.7$s, then switched off, and on again at $t = 1.9$s. From $t = 2.0$s on, $\Delta\phi$ (second panel from top) is continuously ramped up by rotating the MP in upper and lower coil rings with $f = 1$Hz in opposite directions. As a result, two full periods of $\Delta\phi = -180^\circ \ldots 180^\circ$ are completed within one second. The variation of $\Delta\phi$ has significant impact on the plasma properties. At $\Delta\phi = 90 \ldots 180^\circ$, the density is reduced by up to 40% and the ELM energy loss drops from about 25kJ (in the phase without MP) to less than 10kJ. The ELM frequency increases from below 100Hz to about 400Hz. The opposite behavior, a reduction of ELM frequency compared to the no-MP case, is observed in a distinctly separated range of $\Delta\phi = -60^\circ \ldots +40^\circ$. Around $t = 3.0$s, the phase variation is halted at $\Delta\phi = 0^\circ$, resulting in an ELM-free H-mode with associated uncontrolled rise of plasma density, edge pedestal pressure and plasma radiation, terminated by a large ELM at $t = 3.163$s. It should be noted that due to the temporal variation of the MP coil current, there is a significant image current in the passive stabilizing structure onto which the MP coils are mounted. This leads to a phase lag of the MP field at the plasma surface of about 35° with respect to the differential phase of the coil current patterns in upper and lower coils at the frequency of $f = 1$Hz employed during the rotation of the MP field. We can now examine the effect of the density variation induced by variation of $\Delta\phi$ on ELM behavior. Fig. 10 shows data of $\Delta\phi$ scans at low and high q_{95} (orange and pink circles, respectively) highlighted against the background of the full dataset as presented in section 3. One can see that the ELM energy losses during $\Delta\phi$ scans fit to the background data with static or no magnetic perturbation.

In conclusion, all three different methods of varying the plasma density (variation of neutral beam heating, pellet fueling, variation of $\Delta\Phi$) lead to a similar behavior of the ELM energy loss as a function

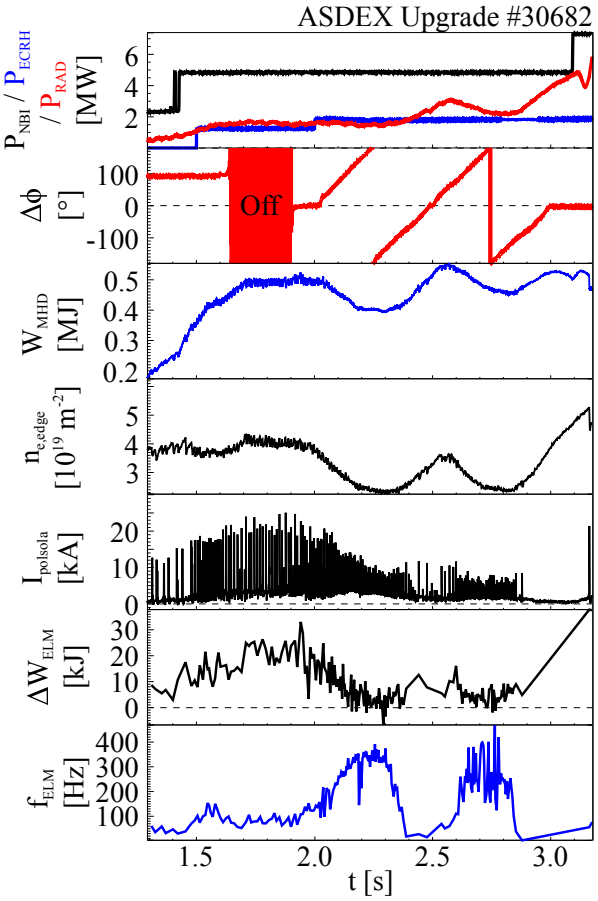

Figure 11. Plasma response during a scan of the differential phase $\Delta\phi$ in discharge #30682 ($q_{95} \approx 3.7$).

of pedestal density.

5. Discussion

5.1. Density scaling or collisionality threshold?

We have seen (section 3) that the ELM energy loss normalized to the pedestal stored energy correlates best with the electron pedestal density both with and without magnetic perturbation. Nevertheless, the collisionality dependence shown in Fig. 6 (a) suggests a collisionality threshold of $\nu^*_{e,PED} < 0.4$ for effective ELM mitigation by magnetic perturbations. Since the ITER-like pedestal collisionality in our experiment will be accompanied with higher pedestal density in ITER, it is important whether both parameters are simultaneously relevant, or whether just one of them can be identified as being critical for controlling the ELM size. While the collisionality as a dimensionless quantity is inherently extrapolative, this is not true for the absolute density, and the popular normalization to the Greenwald limit density [42] is purely empirical in that it does not have a direct theoretical justification in the physics of the hot H-mode pedestal.

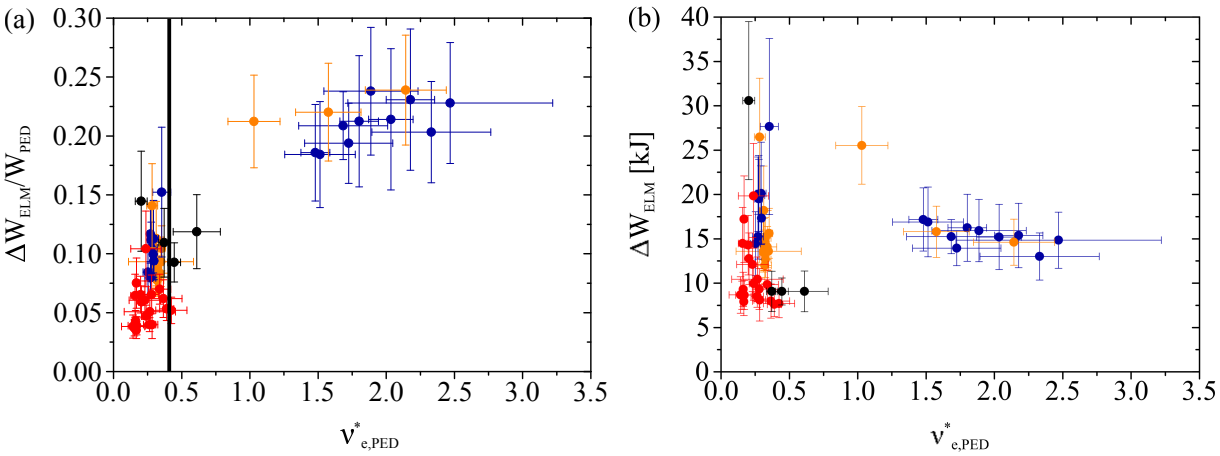

Figure 12. The (a) normalized and (b) absolute ELM energy loss plotted as a function of the collisionality at $n_{e,PED} = 2.75 - 3.25 \cdot 10^{19}\mathrm{m}^{-3}$. Shown are data with magnetic perturbation (● low edge safety factor, ● high edge safety factor) and without magnetic perturbation (● low edge safety factor, ● high edge safety factor).

In an attempt to separate density and collisionality effects, we can select a subset of data in a narrow range of pedestal density, $n_{e,PED} = 2.75 - 3.25 \cdot 10^{19}\mathrm{m}^{-3}$, which exhibits variation of ELM loss energy by a factor of $2-3$ (see Fig. 6 (b)). For this subset, the normalized and absolute ELM loss is shown vs. pedestal collisionality in Fig. 12 (a) and (b), respectively. The variation of collisionality as defined in Eq. 4 originates from using two configurations with different safety factor (indicated by different colours in the figure) and from variations of the effective ion charge number Z_{eff} and pedestal top temperature. One can see that the smallest ELMs occur below a collisionality of about 0.4 (see Fig. 12 (a)). With high edge safety factor, smaller normalized ELM energy loss ($\Delta W_{ELM}/W_{PED} = 0.075 - 0.125$) is obtained at low collisionality, $\nu^*_{e,PED} < 0.4$, than at high collisionality ($\nu^*_{e,PED} > 1.5$, $\Delta W_{ELM}/W_{PED} = 0.18 - 0.27$), although a systematical difference with respect to the low q_{95} configuration ($\Delta W_{ELM}/W_{PED} = 0.025 - 0.075$) remains. Fig. 13 (a) shows the normalized ELM energy loss as a function of the effective ion charge. Here, no clear dependency can be seen and the variation of the impurity content is not responsible for the different normalized ELM losses, since both, small and large ELM losses, are found at low Z_{eff}. A plot of electron pedestal temperature vs normalized ELM energy loss (Fig. 13 (b)) reveals that in the case of the large ELMs at high collisionality the pedestal temperature is very low ($T_{\mathrm{e,ped}} = 0.25 - 0.4\mathrm{keV}$) compared to the case of the small ELMs ($T_{\mathrm{e,ped}} = 0.75 - 0.95\mathrm{keV}$) and, therefore, the difference in the collisionality is mainly due to the difference in the temperature. In Fig. 12 (b) it can be seen that the absolute energy loss due to the ELMs in the high collisionality cases (low pedestal temperature) are not

systematically larger than in the low collisionality cases. The normalization of the ELM energy loss to the pedestal stored energy, which depends on the pedestal temperature according to Eq. 2, is causing those diverging relations. This brings up the question, whether the ELMs at low and high collisionality are effectively different, or in other words, is the normalization of ELM losses to the pedestal stored energy reasonable? Therefore, a subset of data is chosen consisting only of natural ELMs (i.e. without magnetic perturbation) occurring with different energy losses at about constant density. In Fig. 14 one can see the absolute ELM energy loss as a function of the pedestal stored energy and data taken in the same discharge show higher absolute ELM energy losses at higher pedestal stored energy. Since the density is kept about constant, the increase of the stored energy is mainly achieved by an increasing electron and/or ion temperature according to Eq. 2 (note that the volume hardly changes). This indicates that a systematical difference between the ELMs at low and high collisionality (Fig. 12) exists, since even at a three times higher pedestal stored energy the absolute losses are in the same order or even smaller.

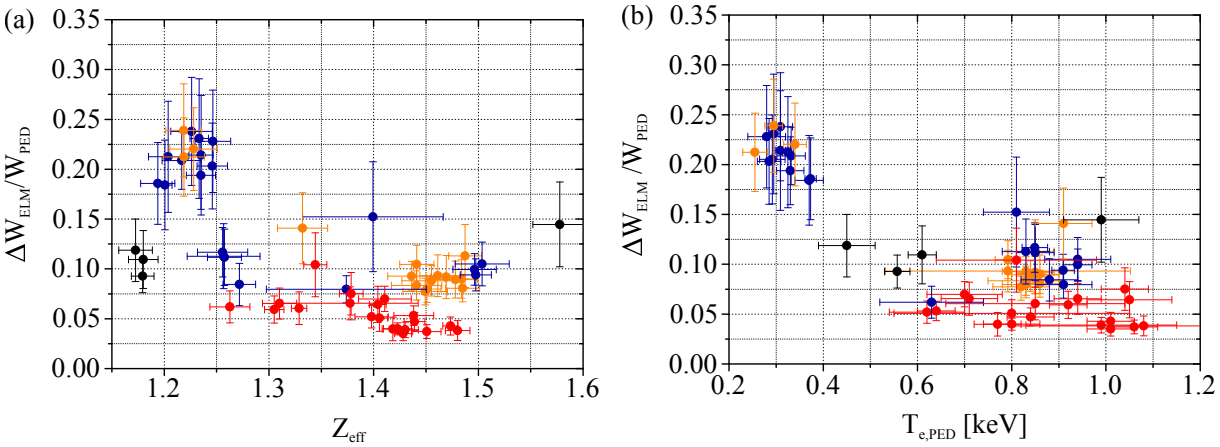

Figure 13. The normalized ELM energy loss as a function of (a) the effective ion charge and (b) the electron pedestal temperature at $n_{e,PED} = 2.75 - 3.25 \cdot 10^{19}\mathrm{m}^{-3}$. Color code of symbols as in Fig. 12.

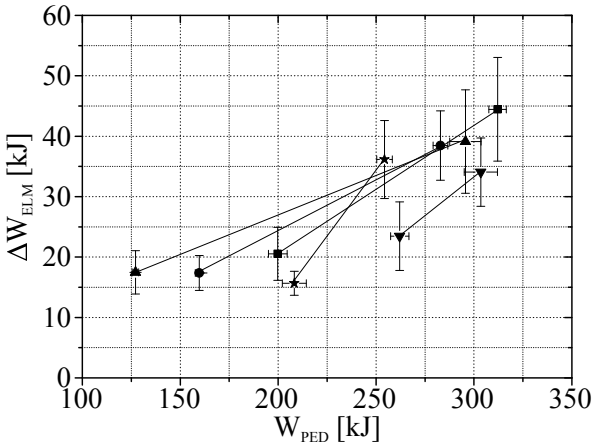

Figure 14. The absolute ELM energy loss as a function of the pedestal stored energy. The data points obtained in the same discharges are linked with solid lines; only low edge safety factor discharges are used.

Operational boundaries of plasma regimes that are distinguished by pedestal parameters such as

ELM stability limits and the L-mode / H-mode boundary can often be depicted in diagrams of pedestal $n_{e,PED} - T_{e,PED}$ [43]. We can include into such a diagram (Fig. 15) the location of $\nu^*_{e,PED} = 0.4$ (for $q_{95} = 3.5$, $R = 1.6$m, $Z_{eff} = 1.1$, $\varepsilon = 0.31$, black curve) and of the empirical pedestal pressure for largest ELMs (red curve). One can see that the highest normalized ELM energy losses above 17.5% of the pedestal stored energy (symbols in yellow, red, and orange colors) can be mostly found at the high density side of a hyperbola of constant pressure $T_{e,PED} \sim 1/n_{e,PED}$ (red curve). This is typical for the pressure-gradient driven ELM instability if the pedestal width remains approximately constant which is the case for the present dataset with fixed plasma shape at low triangularity. ELMs occurring at this boundary at maximum edge pressure are referred to as Type I or compound ELMs [43, 44], if large ELM losses trigger transitions to Type III or L-mode phases. In contrast, the bulk of mitigated ELMs with energy losses lower than 7.5% of the pedestal stored energy (black, dark blue) is spread over a wide temperature range from 0.5 to 1.3keV at low density (1.5 - $3 \cdot 10^{19}$m^{-3}). These low densities have not been reached in ASDEX Upgrade before and are now only accessible due to the "pump-out" associated with magnetic perturbations. This regime is only present at collisionalities lower than $\nu^*_{e,PED} = 0.4$ and overlaps the parameter region of the low collisionality branch of Type III ELMs as found early in DIII-D [44], although in DIII-D no magnetic perturbation by external saddle coils was applied at the time. During the transition from unmitigated ELMs into this regime with small, mitigated ELMs, a transition from Type I to Type III ELMs is therefore likely. Low collisionality Type III ELMs are also found on MAST with and without magnetic perturbations [19]. This observation raises the question if the occurrence of a small ELM type is just a consequence of low pedestal collisionality combined with reduced pedestal pressure, and whether the magnetic perturbation acts solely through the "pump-out" effect which allows, in ASDEX Upgrade, this regime to be attained or whether it has an explicit effect on ELM stability without altering the above-mentioned pedestal parameters. Experimentally, this can be tested in ASDEX Upgrade by separating the magnetic and transport timescales in a discharge where the magnetic perturbation is set up to achieve ELM mitigation and then turned off quickly on a time scale determined by technical boundary conditions, while the pedestal density and pressure recover on a transport time scale of the order of 100 ms. In ASDEX Upgrade, the MP coils are mounted on the passive stabilizing loop (PSL), a massive copper conductor in $n = 0$ saddle loop configuration used to reduce the vertical growth rate of elongated plasmas. Fast transients in the MP coil currents induce mirror currents in the PSL which slow down the shut-off of the magnetic perturbation. This mirror current can be compensated for by a suitably designed MP coil current trajectory such that the normal field at the plasma surface next to the MP coil steps to zero in less than 10 ms. In Fig. 16 the time traces of such a discharge are shown. After turning off the perturbation quickly an ELM-free regime is entered. Because of the missing ELM particle and energy losses and the absence of other transport mechanisms across the H-mode barrier, the pedestal density and temperature increase until a large ELM is triggered, which causes significant energy and particle loss such that after a few trailing ELM-crash events another ELM-free phase is encountered. This sequence recurs until the magnetic perturbation is switched back on, at which time the ELMs become more regular again and clamp the pedestal pressure below that of the large ELM type. This qualitatively different behavior suggests that the magnetic perturbation is an explicit requirement to destabilize moderate ELMs in ASDEX Upgrade at pedestal pressure below the stability limit for large ELMs.

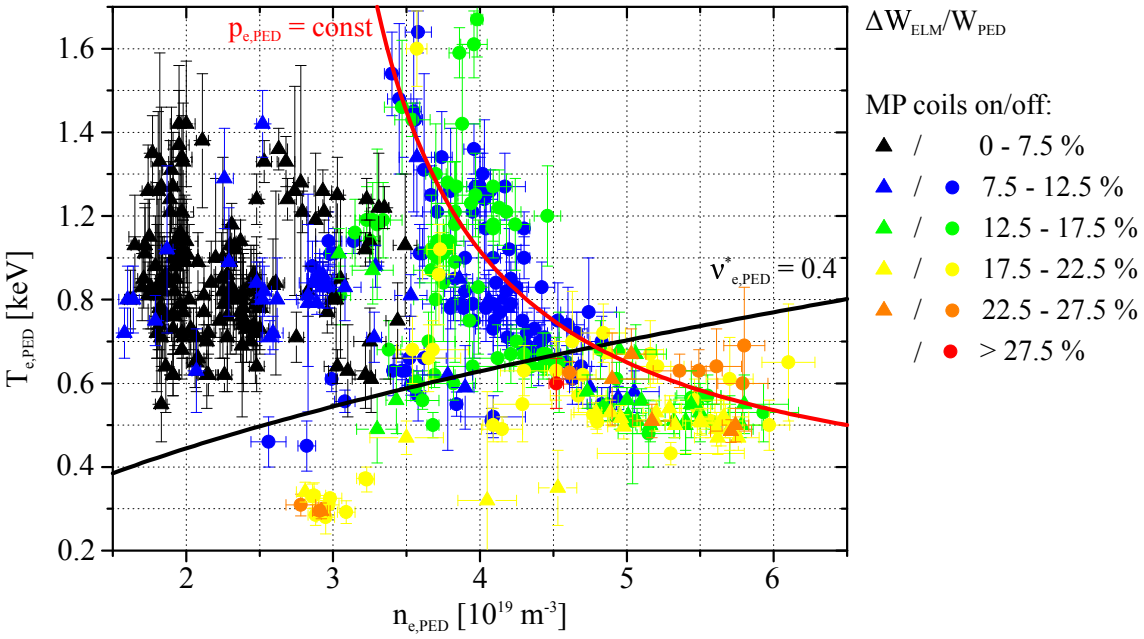

Figure 15. Distribution of the normalized ELM energy losses in a electron pedestal temperature - density diagram. The red curve corresponds to constant pedestal pressure and the black curve is at constant collisionality $\nu^*_{e,PED} = 0.4$ with $q_{95} = 3.5$, $R = 1.6$m, $Z_{eff} = 1.1$, $\varepsilon = 0.31$ and $\ln(\Lambda) = 16$.

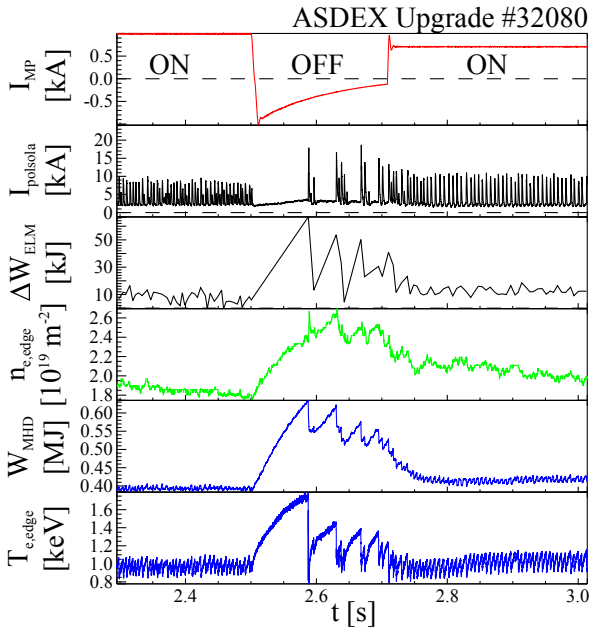

Figure 16. Discharge with a fast shut-off of the magnetic perturbation coils.

5.2. ELM mitigation prospects for ITER

The ITER fusion experiment will have to operate at a electron pedestal collisionality of about $\nu^*_{PED} = 0.1$ and a Greenwald fraction of $n_{e,PED}/n_{GW} = 0.8$ [4]. In the present experiments at ASDEX Upgrade, a comparable pedestal collisionality is achieved, albeit at lower Greenwald density fraction, $15 - 40\%$ of

n_{GW}. In this scenario significant ELM mitigation is found, but at the cost of losing confinement due to the "pump-out" effect. For shot #31128, Fig. 4 shows the time trace of the H-factor H_{98} (confinement time relative to ITER IPB98(y,2) scaling [35]). The ELM energy loss is reduced from $\sim$ 36kJ without MP to less than 5kJ with MP on, corresponding to more than 85% reduction. During this mitigated phase the electron temperature at the pedestal drops by 30% and the density by 45%. The stored energy is reduced by 35%. Without magnetic perturbation, H_{98} is at about 1.2 but drops to 0.7 or less after switching on the perturbation coils. While the reduction of ELM energy loss is encouraging, such a strong reduction of confinement is not compatible with the ITER baseline scenario and may conflict with the objective of $Q = 10$ fusion gain. In section 4 we discussed techniques to regain confinement by increasing the neutral beam injection power or by injecting frozen deuterium pellets. However, methods that are based on at least partial recovery of the electron density showed a concomitant increase of the normalized ELM energy losses.

6. Conclusions

ELM mitigation is achieved with $n = 2$ magnetic perturbation fields in low collisionality and density plasmas at ASDEX Upgrade. The loss in the stored energy caused by ELMs can be reduced by more than 85% to a level where the noise of the stored energy exceeds them. In the entire density range observed, 1.5 to $6.0 \cdot 10^{19}\mathrm{m}^{-3}$, corresponding to 15 to 60% of the Greenwald density, the ELM energy loss normalized to the energy stored in the plasma pedestal is found to correlate with the electron pedestal density such that the smallest ELMs occur at lowest density. The pump-out effect triggered by magnetic perturbations makes those low densities and losses accessible, but at the expense of the confinement, which gets reduced due to lower pedestal pressure. Attempts to compensate the confinement loss with increased neutral beam injection power or by deuterium pellet injection lead to higher ELM losses according to the discovered trend, however, it is implied that one could restore the pedestal pressure by increasing the temperature further at constantly low density. The investigated dataset also suggests an upper collisionality bound at $\nu^*_{e,PED} < 0.4$ for best ELM mitigation. Further studies will be devoted to test the correlation between ELM energy loss and pedestal density and find possible ways to restore the density without compromising ELM mitigation. This is important because at given pedestal temperature, the density controls the pedestal pressure and thereby the total stored kinetic energy of a plasma. Furthermore, high pedestal density operation is important for obtaining the high recycling divertor conditions needed for power exhaust.

Acknowledgement

This work has been carried out within the framework of the EUROfusion Consortium and has received funding from the Euratom research and training programme 2014-2018 under grant agreement No 633053. The views and opinions expressed herein do not necessarily reflect those of the European Commission.

References

[1] Ryter F *et al.* 2009 *Nucl. Fusion* **49** 062003
[2] Leonard A, Herrmann A, Itami K, Lingertat J, Loarte A, Osborne T, Suttrop W, the ITER Divertor Modeling and Database Expert Group and the ITER Divertor Physics Expert Group 1999 *Nucl. Mater.* **266-269**
[3] Federici G, Loarte A and Strohmayer G 2003 *Plasma Phys. Control. Fusion* **45** 1523–1547
[4] Loarte A *et al.* 2003 *Plasma Phys. Control. Fusion* **45** 1549–1569
[5] Loewenhoff T, Linke J, Pintsuk G, Pitts R and Riccardi B 2015 *Nucl. Mater.* **463**
[6] Eich T 2016 *22nd International Conference on Plasma Surface Interactions in Controlled Fusion Devices* vol I11
[7] Liang Y *et al.* 2007 *Phys. Rev. Lett.* **98**
[8] Kirk A *et al.* 2010 *Nucl. Fusion* **50**
[9] Suttrop W *et al.* 2011 *Phys. Rev. Lett.* **106** 225004
[10] Evans T E *et al.* 2004 *Phys. Rev. Lett.* **92**
[11] Jeon Y M *et al.* 2012 *Phys. Rev. Lett.* **109**

[12] Suttrop W *et al.* 2009 *Fusion Engineering and Design* **84** 290–294
[13] Vierle T, Streibl B, Rott M, Seidel U, Herrmann A, Neubauer O, Suttrop W and the ASDEX Upgrade Team 2009 *Fusion Engineering and Design* **84** 1928
[14] Suttrop W *et al.* 2012 *39th EPS Conference and 16th Int. Congress on Plasma Physics* P2.092
[15] Suttrop W *et al.* 2013 *Fusion Engineering and Design* **88** 446–453
[16] Fischer R, Fuchs J C, Rathgeber R M S K, Suttrop W, Willensdorfer M, Wolfrum E and the ASDEX Upgrade Team 2012 *Plasma Phys. Control. Fusion* **54**
[17] Suttrop W *et al.* 2013 *40th EPS Conference on Plasma Physics* P4.117
[18] Suttrop W *et al.* 2014 *25th IAEA Fusion Energy Conference*
[19] Kirk A *et al.* 2015 *Nucl. Fusion* **55**
[20] Jakubowski M 2014 *25th IAEA Int. Conf. on Fusion Energy* EX/P3-47
[21] Willensdorfer M *et al.* (submitted) *Plasma Phys. Control. Fusion* **arXiv:1603.09150**
[22] Ryan D 2014 *Joint EU-US Transport Task Force workshop* (Culham)
[23] Strumberger E, Gnter S and Tichmann C 2014 *Nucl. Fusion* **54**
[24] Orain F *et al.* (accepted) *Nucl. Fusion* **arXiv:1602.07564**
[25] Liu Y *et al.* 2016 *Nucl. Fusion* **56**
[26] Fischer R, Fuchs C J, Kurzan B, Suttrop W, Wolfrum E and the ASDEX Upgrade Team 2010 *Fusion Science and Technology* **58** 675–684
[27] Mlynek A 2010 *Real-time control of the plasma density profile on ASDEX Upgrade* Ph.D. thesis LMU Mnchen
[28] FIscher R, Wolfrum E, Schweinzer J and the ASDEX Upgrade Team 2008 *Plasma Phys. Control. Fusion* **50**
[29] Suttrop W, Peeters A G, the ASDEX Upgrade Team and the NBI group 1997 *IPP Report*
[30] Rathgeber S, Barrera L, Eich T, Fischer R, Nold B, Suttrop W, Willensdorfer M, Wolfrum E and the ASDEX Upgrade Team 2013 *Plasma Phys. Control. Fusion* **55**
[31] Kurzan B, Fischer R, Schneider P A, Suttrop W and the ASDEX Upgrade Team 2011 *38th EPS Conference on Plasma* P4.048
[32] Kurzan B and Murmann H 2011 *Review of Scientific Instruments* **82**
[33] Viezzer E, Pütterich T, Dux R, McDermott R M and the ASDEX Upgrade Team 2012 *Rev. Sci. Instrum.* **83** 103501
[34] Rathgeber S *et al.* 2010 *Plasma Phys. Control. Fusion* **52**
[35] ITER Physics Expert Group on Confinement and Transport, ITER Physics Expert Group on Confinement Modelling and Database, and ITER Physics Basis Editors 1999 *Nucl. Fusion* **39**
[36] Sauter O, Angioni C and Lin-Liu Y R 1999 *Phys. Plasmas* **6** 2834–2839
[37] Myers J L and Well A D 2003 *Research Design and Statistical Analysis* (Lawrence Erlbaum Associates)
[38] Lang P T *et al.* 1996 *Nucl. Fusion* **36**
[39] Valovi M *et al.* 2016 *Nucl. Fusion* **56**
[40] Lang P *et al.* 2012 *Nucl. Fusion* **52**
[41] Paz-Soldan C *et al.* 2015 *Phys. Rev. Lett.* **114**
[42] Greenwald M, Terry J L, Wolfe S M, Ejima S, Bell M G, Kaye S M and Neilson G H 1988 *Nucl. Fusion* **28** 2199
[43] Suttrop W *et al.* 1997 *Plasma Phys. Control. Fusion* **39** 2051–2066
[44] Osborne T H, Gröbner R J, Lao L L, Leonard A W, Maingi R, Miller R L, Porter G D, Thomas D M and Waltz R E 1997 *24th Conference on Controlled Fusion and Plasma Physics* vol 21A